

Anomalous Floquet Phases. A resonance phenomena

Álvaro Gómez-León^{1,*}

¹*Institute of Fundamental Physics IFF-CSIC, Calle Serrano 113b, 28006 Madrid, Spain*

(Dated: December 13, 2023)

Floquet topological phases emerge when systems are periodically driven out-of-equilibrium. They gained attention due to their external control, which allows to simulate a wide variety of static systems by just tuning the external field in the high frequency regime. However, it was soon clear that their relevance goes beyond that, as for lower frequencies, anomalous phases without a static counterpart are present and the bulk-to-boundary correspondence can fail. In this work we discuss the important role of resonances in Floquet phases. For that, we introduce a method to find analytical solutions when the frequency of the drive matches the band gap, extending the well-known high frequency analysis of Floquet systems. With this formalism, we show that the topology of Floquet phases can be accurately captured in analytical terms. We also find a bulk-to-boundary correspondence between the number of edge states in finite systems and a set of topological invariants in different frames of reference, which crucially, does not explicitly involve the micromotion. To illustrate our results, we consider a periodically driven SSH chain and a periodically driven π -flux lattice, showing that our findings remains valid in different systems and dimensions. In addition, we notice that the competition between rotating and counter-rotating terms must be carefully treated when the undriven system is a semi-metal. To conclude, we discuss the implications to experimental setups, including the direct detection of anomalous topological phases and the measurement of their invariants.

CONTENTS

I. Introduction:	1
II. Revisiting the Rabi model:	2
III. 1D Topology: AC driven SSH chain	5
A. High frequency topology	5
B. Derivation of the RWA Hamiltonian	6
C. Topology induced by resonances	8
IV. 2D Topology: AC driven π -flux lattice	9
A. High frequency topology	9
B. Derivation of the RWA Hamiltonian	11
C. Topology induced by resonances	13
V. Conclusions:	15
Acknowledgments	15
References	15
A. General analysis of RWA Hamiltonian	17
B. Additional results for the π -flux lattice	17

I. INTRODUCTION:

Condensed matter has rapidly evolved during the last decades by incorporating concepts from many different areas of physics and mathematics. A quite remarkable

example of this is the field of topological systems, where ideas from topology and particle physics have been borrowed to explain the fundamental properties of certain materials, which could not be understood using the standard classification of phases of matter based on local order parameters [1]. Nowadays, this interplay between topology and physics has been extremely fruitful and extends beyond the frontiers of condensed matter. For example, it is used to predict robust states with applications in quantum computation [2], to explain large-scale climate phenomena [3] or even certain properties of stars [4].

In this plethora of topological phases of matter, non-equilibrium systems play an interesting role. Initially, Floquet topological insulators captured wide attention for being topological systems with an external control [5–9]. However, it was soon realized that their non-equilibrium nature provides richer topology than their equilibrium counterparts [10–13]. For example, Floquet anomalous phases exhibit robust topological edge states with trivial band invariants, something that is utterly impossible in equilibrium systems. Currently, topology in non-equilibrium systems not only involves periodically driven systems, but also dissipative ones [14], which have shown to share extraordinary connections with Floquet systems [15].

On the experimental side, there has been a lot of progress on the observation of topological phenomena, and in particular, Floquet topological insulators have been realized on the surface of topological insulators [16], in cold atoms [17], photonic crystals [18–20] or optical fibers [21, 22], among many others [23].

The study of Floquet phases is a timely research line and anomalous topology represents one of its most myste-

* a.gomez.leon@csic.es

rious and interesting features to explore. Probably, part of this mystery is a consequence of the fundamental differences with static topological insulators and the rather mathematical approach used to characterize anomalous phases. In particular, in Floquet systems quasienergies play a similar role as the energies of static systems, but they are 2π -periodic and this leads to the existence of an additional unequivalent gap between quasienergies, known as π -gap. Also, their topology requires new invariants that involve the micromotion, due to the possibility of band degeneracies during the time evolution [24, 25].

From a more physical point of view, the consequences of these mathematical generalizations to non-equilibrium setups are not clear. One clue to understand the physics behind the emergence of anomalous topology is given by the fact that it only exists out of the high frequency regime. This indicates that the physics of resonances must play a pivotal role, and the transition between the high and the low frequency regime must be related with their existence [26].

In this work, we study the importance of resonance phenomena in Floquet phases, and in particular, in the case of anomalous topology. With this goal in mind, we describe a general procedure to find effective Hamiltonians that faithfully capture the physics of periodically driven systems in the presence of resonances. This approach generalizes well-established high frequency methods and unravels the interplay between resonant and off-resonant processes in the topology of non-equilibrium phases. Also, it accounts for large amplitude modulations, as they play a fundamental role in Floquet engineering.

Our results show that resonances are a crucial ingredient to produce anomalous Floquet phases, and that the phase boundary of the topological phase, as a function of frequency, can be accurately predicted in analytical terms. In addition, we discuss how the symmetries of the driving field affect the existence of phase transitions, by forbidding or allowing exact crossings at particular points of the first Brillouin zone (FBZ). Our results provide a solid methodology to study real situations in experiments, where typically resonant and off-resonant states coexist.

Importantly, we find that the topology of Floquet phases, in the presence of resonances, can be expressed as the combination of the topology of different frames of reference. This allows to subtract the micromotion, which only links different frames of reference, from the topological characterization. In consequence, one can use standard topological invariants over the FBZ, and establish a bulk-to-boundary correspondence between edge states and invariants in each frame of reference.

Finally, in the case of periodically driven semi-metals we also uncover a subtle interplay between rotating and counter-rotating terms. We show that it must be carefully treated to correctly capture both, the renormalization of the off-resonant states and the resonance phenom-

ena.

II. REVISITING THE RABI MODEL:

The Rabi model is one of the most iconic models in quantum physics [27]. It describes, at an elementary level, the interaction between radiation and quantum matter, and as such, it also is a canonical model for non-equilibrium physics.

Beyond its seemingly simple form, the Rabi model for arbitrary field does not have a closed form solution. Despite this, different approximations can provide exact analytical solutions in different regimes of operation, and explain different phenomena such as Rabi oscillations or Floquet engineering. These typically are the rotating wave approximation (RWA) or the high frequency expansions.

In this section we perform a basic analysis of the Rabi model for a two-level system coupled to a radiation field under the dipole approximation, and discuss its analytical solutions and their range of validity. This will be useful to understand the limitations of our approximations in the case of lattice systems coupled to AC fields in the following sections.

The Hamiltonian we consider has the following form:

$$H(t) = \frac{\Delta}{2} \sigma_z + V \cos(\omega t + \varphi) \sigma_x, \quad (1)$$

being ω the frequency of the external field, φ its initial phase, V its amplitude and Δ the splitting of the two-level system (TLS). Importantly, notice that the interaction between the TLS and the field is transversal, which means that the field can drive transitions in the TLS.

In order to explore amplitudes beyond the weak coupling regime, defined by $V \ll \Delta, \omega$, we first perform a transformation to the interaction picture with

$$R_1(t) = e^{-i \int V \cos(\omega t + \varphi) \sigma_x dt}, \quad (2)$$

which leads to a new, time-dependent Hamiltonian:

$$\begin{aligned} H_I(t) &= R_1^\dagger(t) H(t) R_1(t) - i R_1^\dagger(t) \dot{R}_1(t) \\ &= \frac{\Delta}{2} \cos[F(t)] \sigma_z + \frac{\Delta}{2} \sin[F(t)] \sigma_y, \end{aligned} \quad (3)$$

being $F(t) \equiv 2V \sin(\omega t + \varphi)/\omega$. So far, this result is exact, but it is not clear why Eq. (3) is more convenient than Eq. (1), as it is more complex and fully time-dependent. The reason is that the field amplitude dependence is now encoded in the trigonometric functions, which allows us to truncate the Hamiltonian for arbitrary field amplitude. To do this, we just need to apply the well-known Jacobi-Anger expansion of the trigonometric functions in terms of Bessel functions:

$$H_I(t) = \sum_{n=-\infty}^{\infty} \frac{\Delta_n}{2} [\cos(n\omega t + n\varphi) \sigma_z + \sin(n\omega t + n\varphi) \sigma_y] \quad (4)$$

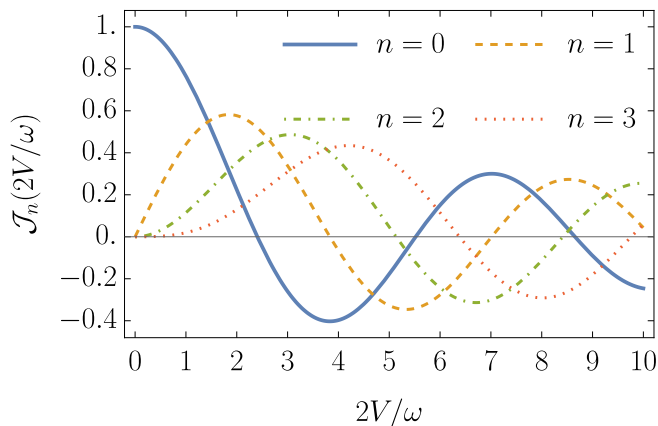


FIG. 1. Bessel functions $\mathcal{J}_n(2V/\omega)$ for $n = 0, 1, 2$ and 3 . They oscillate with slightly different periods and decay for increasing field amplitude.

Notice that each of the Fourier components is renormalized by Bessel functions $\Delta_n = \Delta \mathcal{J}_n(2V/\omega)$, being $\mathcal{J}_n(z)$ the n -th Bessel function of the first kind. This is one of the simplest examples of Floquet engineering, where the parameters of the original Hamiltonian are externally tuned by the applied field [11, 28–30]. Concretely, Eq. (4) is useful because generally, just a few Bessel functions dominate for a particular value of the ratio V/ω , independently of the value of Δ , now encoded in the renormalization factor of each Fourier component.

Also, it is interesting to notice that the original, monochromatic driving in Eq. (1), turns into a drive with an infinite number of harmonics in Eq. (4), when the transformation to the interaction picture is applied. This is a way to understand how the complexity of strong field effects emerge in the form of multi-photon processes, once the transformation to the interaction picture is applied.

At this point it is useful to have some intuition about the behavior of Bessel functions as the ratio V/ω increases. In Fig. 1 one can see that the $n = 0$ Bessel function dominates for small V/ω . As it goes with the time-independent part of the Hamiltonian, this component can be interpreted as field renormalized bands, whose bandwidth tends to zero at large V/ω . This band collapse at large V/ω is well-known, and shows that for very strong drive, bands tend to decouple, in some cases justifying the stroboscopic description of Floquet systems, even at intermediate frequencies. Physically, it can be understood as a large energy shift that brings the system out of resonance. In addition, one can see that the zeroes of the Bessel function correspond to a phenomena known in the literature as coherent destruction of tunneling [31].

The other Bessel functions, $\mathcal{J}_{n \neq 0}(2V/\omega)$, appear with the time-dependent contributions of the effective Hamiltonian. Hence, they can be interpreted as drive terms with an upper-bound value, set by the maximum of the

corresponding Bessel function. Then, it will be reasonable to assume that the largest of all will control the dynamics, specially if its frequency, $n\omega$, is close to the renormalized splitting of the TLS, Δ_0 . Usually the effect of the other components can be accurately captured by means of perturbation theory in powers of $\Delta_{n \neq 0}$, unless the system is very close to resonance with one of them.

For our purposes, we will consider that the field amplitude is such that $|\Delta_1| > |\Delta_{n \geq 2}|$, although one can carry out a similar analysis for a different range of field amplitudes. This allows us to assume that the interaction picture Hamiltonian can be efficiently truncated to the following form:

$$H_I(t) \approx \frac{\Delta_0}{2} \sigma_z + \Delta_1 \sin(\omega t + \varphi) \sigma_y. \quad (5)$$

Equation (5) looks very similar to Eq. (1), with the difference that V is not explicitly present. Its effect is encoded in the renormalized splitting, controlled by the zeroth Bessel function, and in the renormalized coupling to the field, controlled by the first Bessel function (plus an additional $\pi/2$ phase difference in the driving term). Hence, as previously claimed, we can now work with a Hamiltonian similar to the original one, with the advantage that is valid beyond weak field amplitudes.

When the frequency is the dominant energy scale (i.e., in the high frequency regime, $\omega \gg \Delta, V$), the description of the system highly simplifies, because the second term in Eq. (5) can be neglected. The reason for this is that non-zero Fourier components of the Hamiltonian oscillate very rapidly and average to zero over time. This allows to just focus on the stroboscopic dynamics, which is given by the renormalized splitting, Δ_0 .

On the contrary, if the frequency is of the order of the splitting, the time-dependent part of Eq. (5) cannot be neglected and the dynamics must be included. This is the regime of Rabi oscillations, where the solution can be obtained by means of a RWA:

$$H_{\text{RWA}}(t) = \frac{\Delta_0}{2} \sigma_z + \frac{\Delta_1}{2} (e^{i\omega t + i\varphi} \sigma_- + e^{-i\omega t - i\varphi} \sigma_+). \quad (6)$$

To obtain Eq. (6) we have neglected the components proportional to $e^{\pm i(\omega t + \varphi)} \sigma_{\pm}$, which are the counter-rotating terms that are ignored for a RWA. This Hamiltonian can be exactly solved by performing a transformation to a rotating frame $R_2(t) = e^{-i\frac{\omega}{2} t \sigma_z}$, where it becomes time-independent. This results in:

$$\tilde{H} = \frac{\Delta_0 - \omega}{2} \sigma_z + \frac{\Delta_1}{2} (e^{-i\varphi} \sigma_+ + e^{i\varphi} \sigma_-). \quad (7)$$

Now the system can be exactly solved by just finding the eigenvalues of \tilde{H} :

$$\lambda_{\pm} = \pm \frac{1}{2} \sqrt{(\Delta_0 - \omega)^2 + \Delta_1^2}, \quad (8)$$

and its eigenvectors $|\phi_{\pm}\rangle$. The latter can be expressed in the original reference frame as:

$$|\Psi_{\pm}(t)\rangle = R_1(t) e^{-i\frac{\omega}{2} \sigma_z t} e^{-i\lambda_{\pm} t} |\phi_{\pm}\rangle \quad (9)$$

Notice from Eq. (8) that, as the frequency decreases towards Δ_0 , the splitting gets reduced, and precisely at resonance there is an anticrossing controlled by the renormalized coupling strength Δ_1 . Only for a zero of the Bessel function $\mathcal{J}_1(2V/\omega)$ the spectrum exactly closes its gap. Importantly, the RWA is highly accurate at resonance $\omega = \Delta_0$, because resonances are non-perturbative phenomena that mask the perturbative physics underneath. This will be further discussed in the next sections.

Let us now express these results using the language of Floquet theory, as it will be important to link the concept of quasienergies with the eigenvalues in different frames.

Floquet theory can be applied to any system with a periodic time-dependence [32]. In analogy with spatially periodic systems and Bloch theorem, it states that the solutions can be written in terms of conserved quantities called quasienergies and Floquet states, which are periodic in time with the same period as the drive:

$$|\Psi_\alpha(t)\rangle = e^{-i\epsilon_\alpha t}|\Phi_\alpha(t)\rangle, \quad |\Phi_\alpha(t+T)\rangle = |\Phi_\alpha(t)\rangle. \quad (10)$$

Inserting this ansatz in the time-dependent Schrödinger equation, one finds the Floquet equation:

$$[H(t) - i\partial_t]|\Phi_\alpha(t)\rangle = \epsilon_\alpha|\Phi_\alpha(t)\rangle, \quad (11)$$

which is an eigenvalue equation for the Floquet states with Floquet operator $K(t) \equiv H(t) - i\partial_t$ and eigenvalues given by the quasienergies.

Typically in Floquet engineering, due to their time-periodicity, one does a Fourier expansion of the Floquet states, $|\Phi_\alpha(t)\rangle = \sum_n e^{-in\omega t}|\Phi_{\alpha,n}\rangle$, and of the Floquet operator, $K(t)$, which allows to write the eigenvalue equation in terms of Fourier components in an extended Hilbert space, also known as Sambe space [32]. The advantage is that the time-dependence effectively disappears, but the price to pay is that the Floquet operator becomes an infinite dimensional matrix.

Fortunately, in the high frequency regime, the matrix approximately is block diagonal, which allows for simple solutions. However, it is important to stress that the Fourier expansion of the Floquet states is not strictly necessary. It is just specially helpful in the high frequency regime or when the Floquet operator can be block diagonalized [33, 34].

As we are interested in the role of resonances, we directly work with Eq. (11) and solve it for the RWA Hamiltonian in Eq. (6), applying the transformation $R_2(t)$. The solution for the Floquet equation in the original frame reads:

$$|\Phi_\pm(t)\rangle = R_1(t)e^{-i\frac{\omega}{2}\sigma_z t}e^{-i(\lambda_\pm - \epsilon_\pm)t}|\phi_\pm\rangle. \quad (12)$$

Finally, the quasienergies are obtained by requiring that the Floquet state must be T -periodic, $|\Phi_\pm(T)\rangle = |\Phi_\pm(0)\rangle$, which imposes:

$$\epsilon_\pm = \frac{\omega}{2}(2n+1) + \lambda_\pm, \quad \forall n \in \mathbb{Z}, \quad (13)$$

where we have used that $R_1(t+T) = R_1(t)$ and that $R_2(t+T) = -R_2(t)$. Therefore, the Floquet states from Eq. (12) become:

$$|\Phi_\pm(t)\rangle = R_1(t)e^{-i\frac{\omega}{2}\sigma_z t}e^{i\frac{\omega}{2}(2n+1)t}|\phi_\pm\rangle, \quad (14)$$

which are independent of the quasienergy value. Their dependence on the integer n only indicates the redundancy between different Floquet sidebands due to the 2π phase-periodicity. Hence, if one focuses on the zeroth sideband, i.e. in the range $\epsilon_\alpha \in [-\frac{\omega}{2}, \frac{\omega}{2}]$ of Eq. (13), we can finally write the quasienergies and the Floquet states, under the RWA approximation, as:

$$\epsilon_\pm = \pm \frac{\omega}{2} + \lambda_\mp, \quad (15)$$

$$|\Phi_\pm(t)\rangle = R_1(t)e^{-i\frac{\omega}{2}(\sigma_z \pm 1)t}|\phi_\pm\rangle. \quad (16)$$

Crucially, notice that the subscript in the quasienergies, ϵ_\pm , and the eigenvalues of the rotating Hamiltonian, λ_\mp are reversed in our convention. This will be relevant to correctly identify the topological invariants with each band in the examples below.

For illustrative purposes and as a check, let us now focus on the high frequency regime, $\omega \gg \Delta_1$. There, we can perform a series expansion of the eigenvalues λ_\pm and find:

$$\lambda_\pm = \pm \frac{\omega}{2} \mp \frac{\Delta_0}{2} \pm \frac{\Delta_1}{\omega} + \dots, \quad (17)$$

which simplifies the quasienergies to:

$$\epsilon_\pm = \pm \frac{\Delta_0}{2} \mp \frac{\Delta_1}{\omega} + \dots \quad (18)$$

This result is in agreement with the standard high frequency analysis of the original Hamiltonian in Eq. (1) using a Magnus expansion [35], confirming the correctness of our expressions in that regime. In addition, our result is more general, as it is valid also at resonance. Hence, we can use this approach to explore the behavior of the system as the frequency is decreased from the high frequency regime to the resonant one.

To confirm this, we plot in Fig. 2 a comparison between the exact quasienergies and those in Eq. (13) for the zeroth sideband and different field amplitudes. The agreement is excellent not only at the high frequency regime, but also at frequencies below the original resonance, $\omega = \Delta$. Furthermore, the quasienergies are captured in both, the weak coupling (red) and the strong coupling regime (blue).

Importantly, remember that the non-perturbative field amplitude V produces a renormalization of the bands via the Bessel functions. Then, the frequency value at which the actual resonances can happen is now obtained from the non-linear equation:

$$\omega = \Delta \mathcal{J}_0(2V/\omega). \quad (19)$$

The solution of Eq. (19) provides the value at which the frequency matches the renormalized splitting of the RWA

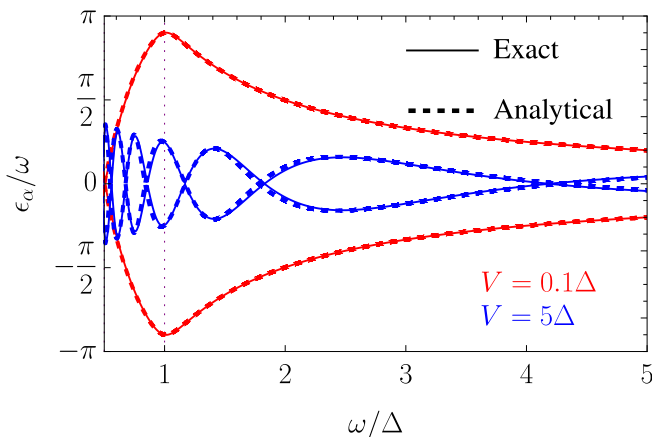


FIG. 2. Comparison between the exact (solid) and the analytical quasienergies (dashed), as a function of frequency and for $V = 0.1\Delta$ (red) and 5Δ (blue). The vertical dotted line indicates the value $\omega = \Delta$.

Hamiltonian, Δ_0 . However, the eigenvalues still have a contribution proportional to $\Delta_{n \neq 0}$ [see Eq. (8)], which due to the incommensurability of the zeroes of the different Bessel functions, will typically lead to an anticrossing of the eigenvalues at zero, or equivalently, to an anticrossing of the quasienergies in the π -gap (i.e., the gap separating neighboring sidebands). That is why in Fig. 2, the weak coupling case shows a small splitting at the π -gap (red).

In addition, the strong coupling case $V = 5\Delta$ is also well-captured, despite of the important contribution from Bessel functions $\mathcal{J}_{n \geq 2}(2V/\omega)$. The reason for this is that the large renormalization of the bands by $\mathcal{J}_0(2V/\omega)$ largely reduces the gap size and one must go to even smaller frequencies to reach resonance. Hence, the system remains in the high frequency regime and the eigenvalues are well-approximated by the first term of Eq. (18). In general we find that the analytical solution starts to fail when ω is of the order of $\Delta_0/2$, which corresponds to the case where the first harmonic, 2ω , becomes resonant. In that situation it is required to use a different effective Hamiltonian with $\mathcal{J}_2(2V/\omega)$ instead of $\mathcal{J}_1(2V/\omega)$. Also, we find that the case $V \sim \Delta$ is generally the most difficult regime to capture.

As a summary of this introductory section, we have shown that the combination of a transformation to the interaction picture with a RWA allows to obtain quite general analytical expressions for the Floquet states and the quasienergies, valid for a wide range of driving regimes. Now we move on to spatially extended systems, and generalize the previous approach to the case of bands with a dispersion relation.

III. 1D TOPOLOGY: AC DRIVEN SSH CHAIN

Lattice systems in condensed matter describe a wide number of physical models, and when coupled to artificial fields [36, 37], it is known that their properties can be externally controlled, giving rise to the field of Floquet engineering [6–8, 11, 12, 25, 30, 38].

Among them, two-band models are some of the simplest cases where non-trivial topology can be present, and when driven out of equilibrium, transitions between the valence and the conduction band can affect the topology. The conditions for resonant transitions are that the driving field must couple the two bands, and that the frequency must be close to their energy difference.

In contrast with the Rabi model previously analyzed, the energy splitting in lattice models generally depends on the quasi-momentum \mathbf{k} , due to the dispersive nature of the bands. This is important because, for a fixed frequency, now there will simultaneously be states that are resonant and off-resonant with the drive [39].

A perfect combination of topology in one-dimension for a two-band model with a driving that introduces topological changes is found in the Su-Schrieffer-Hegger (SSH) chain [40]. When it is periodically driven in time [11, 41, 42], one finds that the quasienergies can exhibit topological edge states in both gaps. Furthermore, if the hopping amplitudes are periodically modulated in a chirally symmetric way, it is possible to find regions of the phase diagram where 0-gap and π -gap edge states can coexist [43–45]. In that case, the Zak phase of the Floquet bands or winding number (if expressed in units of π), is trivial. However, it is known that one can define a new pair of topological invariants adapted to Floquet phases, and topologically characterize this anomalous phase [46], predicting the existence of edge states. We will refer to this situation, which does not have a static analog, as the anomalous topological phase of this 1D Floquet Hamiltonian. Now we discuss the topology in different frequency regimes.

A. High frequency topology

The Hamiltonian for the periodically driven SSH chain can be written as:

$$H(t) = \sum_j \left(J_1(t) b_j^\dagger a_j + J_2(t) a_{j+1}^\dagger b_j + \text{h.c.} \right), \quad (20)$$

with $J_1(t) \equiv J + v(t)$, $J_2(t) \equiv J' - v(t)$ and the modulation of the hopping $v(t) = 2V \cos(\omega t)$, being V the modulation amplitude and ω its frequency.

This time modulation is different to the one typically assumed for light-driven Hamiltonians [11, 42]. The system can be thought as a dimerized lattice with sites linearly coupled by springs, and with the hopping of particles directly proportional to the distance between them. When the sites in one sublattice are linearly shifted from

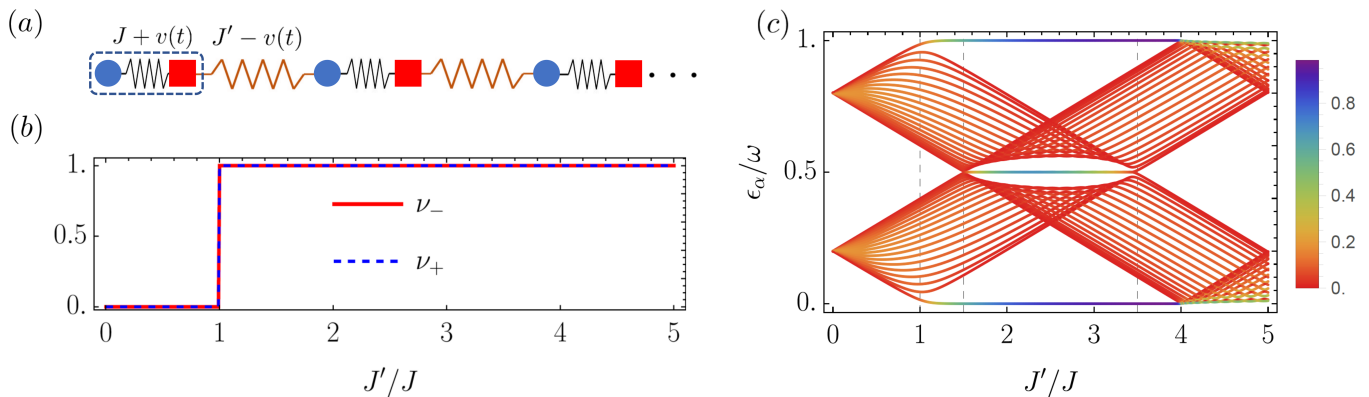


FIG. 3. (a) Schematic representation of the periodically driven dimers chain with a chiral symmetric time modulation of the hoppings. The dashed rectangle indicates the unit cell, and the time-modulation linearly enhances/reduces each hopping by changing the separation between sites. (b) Winding number for each band as a function of the dimerization ratio J'/J . (c) Quasienergy spectrum for the driven chain with OBC, as a function of J'/J . Notice that the spectrum is centered at the π -gap. Parameters: $\omega = 5J$, $V = 0.2J$ and 20 sites. The color code indicates the localization of the states towards the boundaries.

their equilibrium position, one hopping is enhanced the same amount as the other one is reduced. This modulation is harmonically changed with frequency ω , related with the stiffness of the springs (see Fig. 3, panel (a), for an schematic) [47].

To analyze the system in simple theoretical terms, we first consider the case of periodic boundary conditions (PBC). In that case, the system is translationally invariant and we can Fourier transform to momentum space. In the basis $(a_k, b_k)^T$, the time-dependent Hamiltonian matrix reads:

$$H_k(t) = \begin{pmatrix} 0 & J_1(t) + J_2(t)e^{-ik} \\ J_1(t) + J_2(t)e^{ik} & 0 \end{pmatrix}. \quad (21)$$

In this case the high frequency topology is easy to capture. To lowest approximation, the effective stroboscopic Hamiltonian is given by that of the average Hamiltonian $H_0(k) \equiv \int_0^T H_k(t) dt/T$ [35], which in this case coincides with the undriven SSH chain. Due to the chiral symmetry in Eq. (21), the Zak phase is quantized and can be calculated as:

$$\gamma_\pm = \int_{-\pi}^{\pi} \langle \pm | i\partial_k \log \Lambda(k) | \pm \rangle dk, \quad (22)$$

with $\Lambda(k)$ the transformation matrix of eigenvectors which diagonalizes $H_0(k)$ and $|\pm\rangle$ the unit vectors $(1, 0)$ and $(0, 1)$, respectively. Its calculation is straightforward using a contour in the complex plane, and due to its relation with the winding number of the system $\nu_\pm = \gamma_\pm/\pi$, we can directly write $\nu_\pm = \Theta(J'/J - 1)$, as shown in Fig. 3, panel (b). Notice that the winding number for the two bands is identical.

To confirm our prediction we show in Fig. 3, panel (c), the exact quasienergies centered at the π -gap, for the case of OBC. It can be seen that, for our choice with

$\omega = 5J$, the system for small J'/J is in the high frequency regime, because the frequency is larger than the bandwidth $2(J + J')$. Then, at $J' = J$, a topological edge state appears at the 0-gap, as predicted by the winding number of the stroboscopic Hamiltonian. For larger values of J' , the bandwidth continues increasing, until at $J' = 1.5$ we abandon the high frequency regime, because it matches the drive frequency ω and the π -gap closes. This produces an additional localized edge state in the π -gap. Interestingly, when the edge states in both gaps are simultaneously present, the calculation of the winding number results in a zero value.

In the following, we discuss the appearance of this edge state, show its topological origin and its relation with a particular resonance with states at $k = 0$.

B. Derivation of the RWA Hamiltonian

As seen above, precisely at the resonance condition, the system develops additional edge states in the π -gap. This indicates that resonances play a crucial role in the anomalous topology of Floquet phases. To further understand this process, we will derive a RWA Hamiltonian for the driven SSH chain, to capture the main mechanism causing the topological phase transition.

We consider the Hamiltonian with PBC and separate the driven and static parts of the Hamiltonian:

$$H_k(t) = H_0(k) + V(k, t). \quad (23)$$

As for a resonance the transitions between valence and conduction bands is important, we will first diagonalize the static part of the Hamiltonian:

$$\Lambda^\dagger(k)H_0(k)\Lambda(k) = D(k), \quad (24)$$

with $D(k)$ a diagonal matrix with the energies $E_\pm(k) = \pm\sqrt{J^2 + J'^2 + 2JJ'\cos(k)}$ as entries, and the unitary

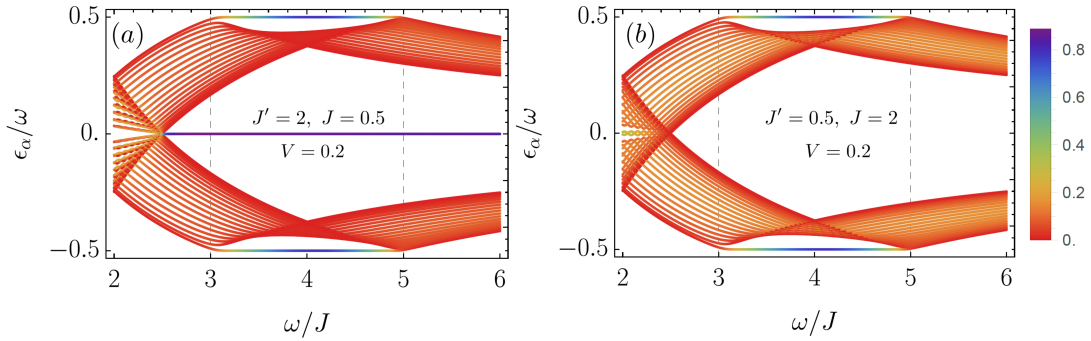


FIG. 4. Quasienergies for OBC as a function of frequency and centered at the 0-gap. The color code indicates the localization towards the edges. (a) Spectrum for the case of a topological phase at high frequency. (b) Spectrum for the case of a trivial phase at high frequency. The critical points are independent of the high frequency topology and only depend on the resonances at $\omega = 2|J \pm J'|$.

transformation matrix $\Lambda(k)$, with its columns given by the eigenvectors of $H_0(k)$. Notice that $\Lambda(k)$ encodes all the information about the topology of the undriven SSH chain in its k -dependence, and that the energies $E_{\pm}(k)$ provide a definition for the bands where the resonances will take place.

Next, we rewrite $H_k(t)$ in this eigenstates basis:

$$\hat{H}_k(t) \equiv \Lambda^\dagger(k) H_k(t) \Lambda(k) = D(k) + \hat{V}(k, t), \quad (25)$$

with $\hat{V}(k, t) = \Lambda^\dagger(k) V(k, t) \Lambda(k)$ now being a complicated matrix with all its entries different from zero. To simplify its form, one needs to remember how different physical processes are related with the various entries. For example, the diagonal part does not couple different bands and corresponds to a time-modulation, independent for each band, that only modifies the phase acquired over time by each eigenstate, in a non-linear way. Off-diagonal elements are more relevant and they can be separated in two types: the ones that can produce resonances and the ones that cannot. For a two-band model they are easy to identify, as the resonant ones coincide with the rotating terms of the Rabi model:

$$\hat{V}_R(k, t) = \hat{V}(k)^{2,1} \sigma_- e^{i\omega t} + \hat{V}(k)^{1,2} \sigma_+ e^{-i\omega t}, \quad (26)$$

with j and l indicating the row and column of the matrix $\hat{V}(k)^{j,l}$, respectively. Notice that in Eq. (26) we have already separated from $\hat{V}(k, t)^{j,l}$ the frequency components that results in resonances. That is why the matrix elements of $\hat{V}(k, t)$, indicated by $\hat{V}(k)^{j,l}$, are time-independent. In more complex cases with a larger number of bands the resonant terms can be systematically identified with the secular terms of the first order correction in time-dependent perturbation theory [48, 49]:

$$\int e^{iD(k)t} \hat{V}(k, t) e^{-iD(k)t} dt. \quad (27)$$

Finally, all the remaining time-dependent, off-diagonal terms of $\hat{V}(k, t)$ can be identified with counter-rotating

terms. Crucially, their contribution is small near resonances and their effect can be incorporated by means of perturbation theory later on. For this reason, we will keep to lowest order the RWA terms only, and define our approximate Hamiltonian for the SSH chain as:

$$H_{\text{RWA}}(k, t) = D(k) + \hat{V}_R(k, t). \quad (28)$$

In this particular case it is easy to write the explicit form of the RWA terms (they fulfill $\hat{V}(k)^{1,2} = [\hat{V}(k)^{2,1}]^*$) as:

$$\Gamma(k) \equiv \hat{V}(k)^{1,2} = \frac{i(J + J')V \sin(k)}{\sqrt{J^2 + J'^2 + 2JJ' \cos(k)}}, \quad (29)$$

which vanish for $V \rightarrow 0$, as expected, but also at $k = n\pi$ with $n \in \mathbb{Z}$.

We can exactly solve the time-dependent Schrödinger equation for $H_{\text{RWA}}(k, t)$ in a similar way as for the Rabi model, by just applying a time-dependent transformation $R(t) = e^{-i\frac{\omega}{2}t\sigma_z}$. This results in the following *time-independent* Hamiltonian in the rotating frame:

$$\tilde{H}(k) = \begin{pmatrix} E_+(k) - \frac{\omega}{2} & \Gamma(k) \\ \Gamma(k)^* & \frac{\omega}{2} - E_+(k) \end{pmatrix}. \quad (30)$$

Notice its similarity with Eq. (7), where the frequency also changes the gap of the unperturbed bands. The eigenvalues are given by:

$$\tilde{E}_{\pm}(k) = \pm \sqrt{\left(E_+(k) - \frac{\omega}{2}\right)^2 + |\Gamma(k)|^2}, \quad (31)$$

and one can see that, as in the Rabi model, the rotating terms produce anti-crossings at the resonance condition:

$$\omega = 2\sqrt{J^2 + J'^2 + 2JJ' \cos(k)}. \quad (32)$$

In contrast with the Rabi model, at particular points of the FBZ given by $k = n\pi$, the eigenvalues become exactly degenerate and the gap closes. This condition is a direct consequence of the symmetry of the driving protocol, which is what allows the coexistence of 0-gap and

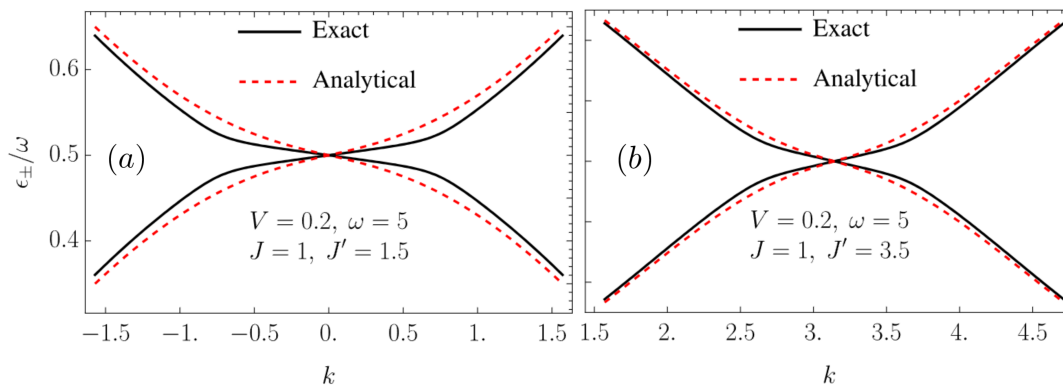


FIG. 5. Comparison between the exact and the analytical quasienergies for the system with PBC at resonance for $J' = 1.5$ (a) and 3.5 (b). The π -gap closes at high symmetry points $k = 0$ and π . Notice the scale of the plot where differences are enhanced.

π -gap edge states. For this reason, more general driving protocols might fail to produce a robust anomalous phase in the driven SSH chain.

To demonstrate this explicitly, let us first find the condition for a gap closure as a function of frequency. As it must happen at the particular points $k = n\pi$, because only there $\Gamma(k)$ in Eq. (31) vanishes, the resonance condition in the first term simplifies to $\omega = 2E_+(n\pi)$. In particular, for each case we obtain:

$$\omega = \begin{cases} 2(J + J') & \text{for } k = 0 \\ 2|J - J'| & \text{for } |k| = \pi \end{cases} \quad (33)$$

These two values perfectly predict the closures of the π -gap in Fig. 3, first at $J' = 1.5$ and then at $J' = 3.5$, linked with the appearance and disappearance of the edge states in that gap. Importantly, their position does not change for moderate values of V , confirming that the resonance mechanism is what controls the gap closure and the topological phase transition.

Eq. (33) also seems to indicate that the gap closure does not depend on the dimerization phase. Hence, the appearance/disappearance of edge states in the π -gap must be independent of the topology of the high frequency stroboscopic Hamiltonian. We confirm that this is indeed the case, as shown in Fig. 4, panels (a) and (b). One can see that as the frequency is reduced, the gap closures are perfectly predicted by Eq. (33) for both cases, independently of the original dimerization phase, with the corresponding appearance/disappearance of edge states. This feature seems to indicate that the presence of edge states in each gap can be independently studied, in agreement with the definition of invariants in Floquet systems for each gap [19, 46].

In Fig. 5, panels (a) and (b), we compare the exact quasienergy spectrum for PBC, with the analytical one from Eq. (31). One can see their good agreement, and importantly, confirm that the rotating terms dominate at the resonances, because the ratio between counter-rotating and rotating terms, or equivalently, the disagree-

ment with the exact result gets reduced as k approaches $k \rightarrow n\pi$.

C. Topology induced by resonances

Finally, as we have analytical expressions that perfectly predict the appearance of edge states in the 0- and π -gap, let us analyze the Zak phase of the Floquet states. In the original frame of reference their expression simply is:

$$|\Phi_{\pm}(k, t)\rangle = \Lambda(k) e^{-i\frac{\omega}{2}t(\sigma_z \mp 1)} |\phi_{\pm}(k)\rangle, \quad (34)$$

where notice that the only difference with the Floquet states in the Rabi model is the additional k -dependence in both, the transformation $\Lambda(k)$ and the eigenstates of $\hat{H}(k)$ in Eq. (30), $|\phi_{\pm}(k)\rangle$.

Importantly, as the Floquet states are periodic in both, k and t , they are the ones that must encode the topological properties, and not the solutions to the Schrödinger equation in Eq. (9) [50]. Furthermore, as the π -gap closure is captured by the rotating frame Hamiltonian, we expect that $|\phi_{\pm}(k)\rangle$ encodes the π -gap topology. In contrast, the 0-gap topology is related with the high frequency regime, and then, it must be partially encoded in the transformation $\Lambda(k)$.

To see this explicitly, we calculate the Zak phase:

$$\gamma_{\pm}(t) = \int_{-\pi}^{\pi} \langle \Phi_{\pm}(k, t) | i\partial_k | \Phi_{\pm}(k, t) \rangle dk, \quad (35)$$

and if we use Eq. (34), we can separate the result in two contributions:

$$\gamma_{\pm}(t) = \int_{-\pi}^{\pi} \langle \phi_{\pm}(k, t) | i\partial_k \log \Lambda(k) | \phi_{\pm}(k, t) \rangle dk + \tilde{\gamma}_{\pm}, \quad (36)$$

where we have defined the *time-independent* Zak phase in the rotating frame:

$$\tilde{\gamma}_{\pm} = \int_{-\pi}^{\pi} \langle \phi_{\pm}(k) | i\partial_k \phi_{\pm}(k) \rangle dk, \quad (37)$$

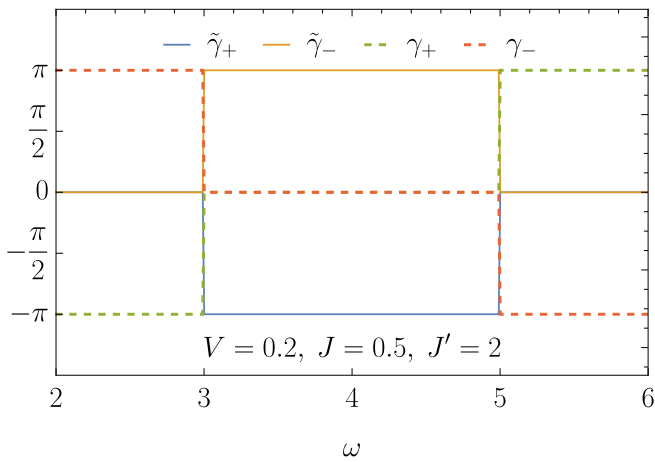


FIG. 6. Zak phase of each Floquet state as a function of the frequency (dashed), for arbitrary time t . The solid lines correspond to the contribution from the rotating frame Hamiltonian. Parameters: $V = 0.2$, $J = 0.5$ and $J' = 2$.

and the first term in Eq. (36), where the original Berry connection is now evaluated with the Floquet states in the eigenstates basis $|\phi_{\pm}(k, t)\rangle = e^{-i\frac{\omega}{2}t(\sigma_z \mp 1)}|\phi_{\pm}(k)\rangle$. In Fig. 6 we plot the value of the Zak phase as a function of frequency, for an arbitrary time t (dashed lines), as well as the value of the Zak phase in the rotating frame (solid lines). The calculation has been done by discretizing the momentum and computing the total angle rotated by the overlap function $\langle \Phi_{\pm}(k, t) | \Phi_{\pm}(k + \delta k, t) \rangle$, as the FBZ is swept.

This is an interesting result, first because one can see that the Zak phase in the rotating frame, $\tilde{\gamma}_{\pm}$, is quantized, it always vanishes in the high frequency regime and only changes its value when the π -gap closes its gap due to a resonance. Hence, it perfectly predicts the existence of edge states in the π -gap and endows them with a topological origin. Second, the first contribution to Eq. (36) that we call $\bar{\gamma}_{\alpha}$, is clearly linked to that of the high frequency regime Zak phase [cf. Eq. (22)], but now evaluated for the Floquet states instead [51]. This produces an important difference, as now the Zak phase in the high frequency regime has opposite sign for each eigenstate. This makes the total Zak phase vanish in the resonant frequency range, $\omega \in [3, 5]$ in Fig. 6, because the rotating frame contribution has opposite sign. Hence, we can write:

$$\gamma_{\alpha} = \bar{\gamma}_{-\alpha} + \tilde{\gamma}_{-\alpha}. \quad (38)$$

Importantly, for this to be obtained, one must be careful with the difference in the band index between eigenstates of the rotating frame Hamiltonian and quasienergies, as shown in Eq. (16). As a check, we have calculated the exact Floquet states from the full, periodically driven SSH Hamiltonian and found perfect agreement for the Zak phase with our analytical results.

In summary, our results explain why the calculation of the Zak phase in a resonant frequency range results

in a topologically trivial band (i.e., with winding number zero), but still display topological edge states in both gaps. We have shown that the topological invariant actually corresponds to the sum of two contributions:

- An invariant from the rotating frame Hamiltonian which captures the resonance mechanism and characterizes the π -gap topology.
- Another invariant from the original lab frame Hamiltonian which captures the high frequency topology and characterizes the 0-gap topology.

Notice that this identification between frames of reference and gaps avoids the use of logarithm branch-cuts, typically present in the study of Floquet systems. In our case, we have access to a rotating frame invariant, which in combination with the invariant from the Floquet bands, allows to fully determine the topology of the system. It is interesting that the topological characterization does not require to explicitly make use of the micromotion, although it shows that is crucial, because it is what separates the different frames of reference. This simplifies the mathematical analysis, as the base manifold is just spanned by the FBZ.

A natural question to ask is if these results are only valid for the present case of a 1D topological system with chiral symmetry. In the following section we discuss two-dimensional systems and show that a similar analysis can be performed where the general conclusions drawn from the 1D case still hold.

IV. 2D TOPOLOGY: AC DRIVEN π -FLUX LATTICE

Anomalous Floquet topological phases are typically associated with two-dimensional systems, where the Chern number of the quasienergy bands vanishes, but the presence of chiral edge states in the two inequivalent gaps indicates some underlying topology [25]. Their topological analysis can be carried out in terms of a winding number $W[U_{\epsilon}]$ [10], which is evaluated over the (\mathbf{k}, t) manifold. A non-vanishing value indicates that the micro-motion is a fundamental ingredient for their characterization [24].

In this section we generalize our previous approach to two dimensions and show that resonances still control the topological phase transitions in the π -gap. We also demonstrate that the Chern number of the Floquet bands still corresponds to the sum of invariants in different frames, making our description valid to describe Floquet topological phases beyond high frequency, in two-dimension.

A. High frequency topology

We consider a square lattice with alternating hopping along the vertical axis (see Fig. 7, panel (a)), for

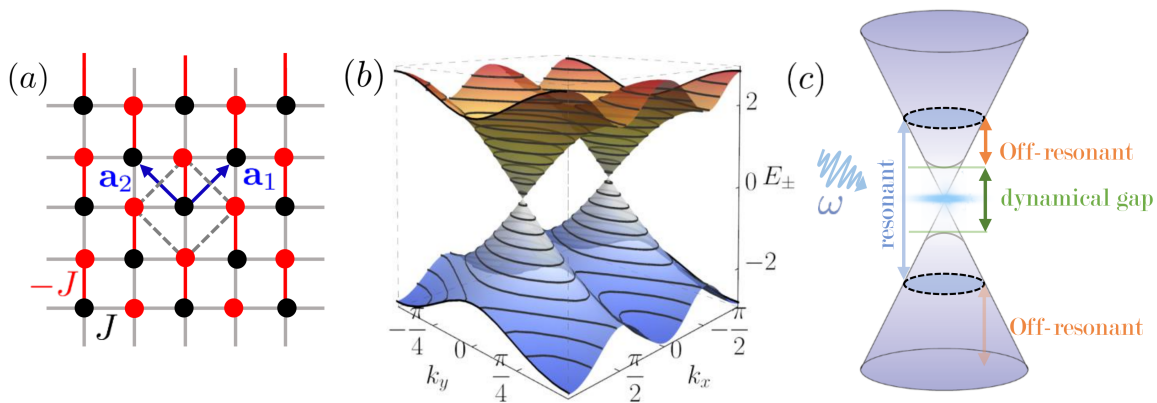


FIG. 7. (a) Schematic of a π -flux lattice with alternating hopping $\pm J$ along the vertical axis, unit vectors $\mathbf{a}_{1,2}$ and lattice constant $a = 1$. (b) Band structure of the undriven system and its pair of Dirac cones at $\mathbf{k} = \pi(\pm 1, 0)/2$. (c) Schematic description of a driven Dirac cone and the relevant energy scales.

a schematic description). This bipartite lattice can also be interpreted as a square lattice with a magnetic flux of half a quanta along the vertical axis [52, 53].

The band structure has two unequivalent Dirac cones and, in the absence of driving, its topology is similar to the one of a honeycomb lattice, with two topological Dirac points protected by symmetry [54]. For this reason, when OBC are considered, the spectrum displays zero-energy modes localized at the edges, whose appearance depends on the particular boundary under consideration [55].

An advantage of the π -flux with respect to other lattices, such as the honeycomb, is that when coupled to an AC field via the Peierls substitution, its Floquet operator is quite direct to write. On top of this, the π -flux lattice has been less studied in the literature, which is why we think this model is interesting to exemplify our findings and perform a full analysis of its Floquet physics.

When a high frequency AC field is applied to a Dirac semi-metal such as this one, it is possible to open a Haldane gap and generate chiral edge states in the 0-gap [6, 7, 9, 30]. As the frequency is reduced, the gap between unequivalent Floquet sidebands can be closed and additional edge states in the π -gap might also appear, which can be propagating or counter-propagating [12]. Importantly, the Chern number of the Floquet bands changes as the frequency is reduced, and typically its value does not coincide with the number of edge states in the sample, invalidating the bulk-to-edge correspondence of static topological insulators [15]. This feature indicates that anomalous topological phases are possible. The relation between bulk invariants and edge states is only recovered when a generalization of the standard classification includes the role of micro-motion [10, 24, 56].

In particular for our case, the Hamiltonian for the un-

driven lattice is given by:

$$H_{\mathbf{k}} = 2J [\cos(k_x)\sigma_x + \sin(k_y)\sigma_y], \quad (39)$$

and its energies simply are $\pm 2J\sqrt{\cos^2(k_x) + \sin^2(k_y)}$, with the two unequivalent Dirac cones located at $\mathbf{k} = (\pm\pi/2, 0)$, as shown in Fig. 7, panel (b). The Peierls substitution, $\mathbf{k} \rightarrow \mathbf{k} + \mathbf{A}(t)$, produces the periodically driven model, and in particular, if we assume a simple time-dependence of the form: $\mathbf{A}(t) = (A_x \sin(\omega t), A_y \sin(\omega t + \varphi))$, it is possible to express the Hamiltonian in terms of its Fourier components:

$$H_{\mathbf{k}} = \sum_n H_{\mathbf{k}}^{(n)} e^{in\omega t}, \quad (40)$$

For that, one just needs to use the Jacobi-Anger identity, which introduces the familiar Bessel functions, and results in:

$$H_{\mathbf{k}}^{(n)} = [e^{ik_x} \mathcal{J}_n(A_x) + e^{-ik_x} \mathcal{J}_{-n}(A_x)] \sigma_x - ie^{in\varphi} [e^{ik_y} \mathcal{J}_n(A_y) - e^{-ik_y} \mathcal{J}_{-n}(A_y)] \sigma_y, \quad (41)$$

with $\mathcal{J}_n(z)$ the n -th Bessel function of the first kind. Notice that the phase difference between components, φ , or polarization, appears only for components with $n \neq 0$. This means that some dynamics is required to define the polarization, as one would expect.

As for the SSH chain in the previous section, a first analysis of the topology can be easily carried-out using a Magnus expansion, which is valid in the high frequency regime. Concretely, it is known that in order to open the Haldane gap, frequency corrections to first order must be considered [8, 12, 57]. In that case the stroboscopic Hamiltonian can be approximated by:

$$\bar{H}_{\mathbf{k}} \approx H_{\mathbf{k}}^{(0)} + \sum_{n>0} h_n(\mathbf{k}, \varphi) \sigma_z, \quad (42)$$

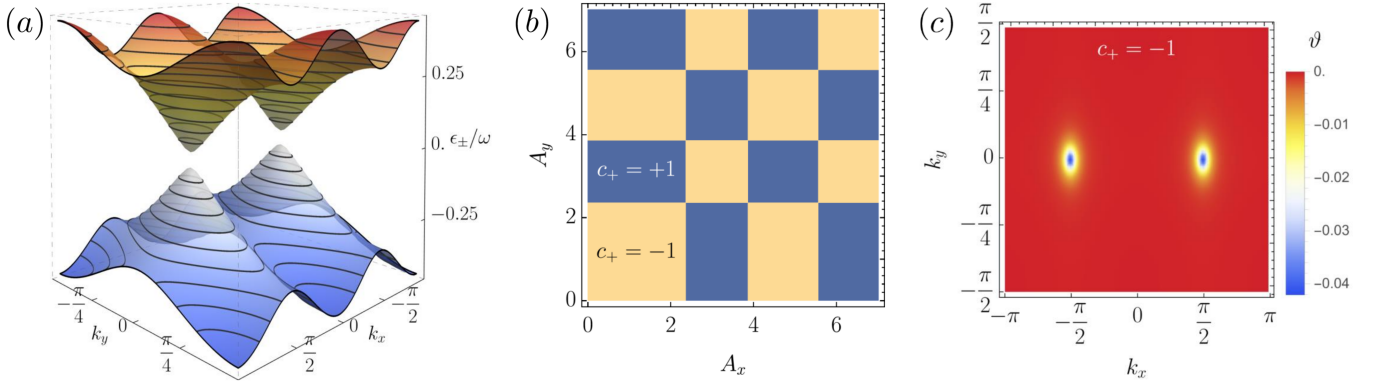


FIG. 8. (a) Quasienergies at high frequency for $A_x = A_y = 0.5$. The mass term opens a topological 0-gap which leads to a non-zero Chern number and to the appearance of edge states. (b) Topological phase diagram as a function of the field amplitude along each axis. (c) Berry flux distribution for the upper quasienergy band highly localized around the Dirac points. Parameters: $\omega = 6J$ and $\varphi = \pi/2$.

with the mass term components $h_n(\mathbf{k}, \varphi) \sigma_z = [H_{\mathbf{k}}^{(n)}, H_{\mathbf{k}}^{(-n)}]/n\omega$, and in particular,

$$h_n(\mathbf{k}, \varphi) \equiv -16J_{x,n}J_{y,n} \sin(k_x) \cos(k_y) \sin(n\varphi) / n\omega \quad (43)$$

for n an odd integer, and

$$h_n(\mathbf{k}, \varphi) \equiv 16J_{x,n}J_{y,n} \cos(k_x) \sin(k_y) \sin(n\varphi) / n\omega \quad (44)$$

for n an even integer. We have also defined $J_{u,n} = J\mathcal{J}_n(A_u)$ as the renormalized hopping along the $u = x, y$ direction. On top of this, if we assume moderate field amplitudes such that the contribution from the first Bessel function is enough to describe the dynamics, the mass term simplifies to:

$$h_1(\mathbf{k}, \varphi) = 16J_{x,1}J_{y,1} \sin(k_x) \cos(k_y) \sin(\varphi) / \omega. \quad (45)$$

Then, the eigenvalues of the stroboscopic Hamiltonian are:

$$\epsilon_{\pm}(\mathbf{k}) = \pm 2\sqrt{J_{x,0}^2 \cos^2(k_x) + J_{y,0}^2 \sin^2(k_y) + h_1(\mathbf{k}, \varphi)^2} \quad (46)$$

which show that the driving can introduce spatial anisotropy in the hopping, but more importantly, that the mass term adds an additional contribution to the eigenvalues which is maximized at the original Dirac points $\mathbf{k} = (\pm\pi/2, 0)$, opening the 0-gap. Figure 8, panel (a), shows the exact quasienergies for circular polarization in the high frequency regime, demonstrating the opening of the 0-gap. The agreement with Eq. (46) is excellent, as far as the frequency is the dominant energy scale and the quasienergies in different sidebands are widely spaced.

To study the topology of the dynamically induced gap in the high frequency regime we can apply the tools of static systems [58, 59]. Then, as the system lacks any of the relevant symmetries for topology and is two-dimensional, we can conclude that its topology is characterized by a Chern number. Its calculation can be carried

out analytically [60], and we find:

$$c_{\pm} = \mp \text{sgn}[J_{x,0}J_{y,0}] \text{sgn}[J_{x,1}J_{y,1} \sin(\varphi)]. \quad (47)$$

In Fig. 8, panel (b), we show the phase diagram as a function of the field amplitude along each axis. One can clearly see that the topological changes are produced by the zeroes of the Bessel functions $\mathcal{J}_0(A_{x,y})$ and $\mathcal{J}_1(A_{x,y})$. This mechanism to create a topological phase in a semi-metal using a high frequency AC field is analogous to the one reported in previous studies. However, the phase diagram and its dependence on the external field parameters is particular to this lattice.

Importantly, notice that in order to find the mass term in Eq. (45), we have not made a distinction between rotating or counter-rotating terms, because at high frequency both are expected to contribute equally. This will be of crucial importance in the next section.

B. Derivation of the RWA Hamiltonian

We now ask about the effect of lowering the frequency and the possibility to obtain a RWA Hamiltonian that captures the physics dominating the topological changes.

First, we assume moderate field amplitudes such that the full Hamiltonian can be truncated to the contributions proportional to the zeroth and the first Bessel functions only. Next, notice that in contrast with the SSH chain, we have two choices for the static band structure of the approximate Hamiltonian [61]: we can consider $H_{\mathbf{k}}^{(0)}$, which describes a semi-metallic phase with renormalized hopping. In that case the full time-dependent Hamiltonian is:

$$H_{\mathbf{k}}(t) \approx H_{\mathbf{k}}^{(0)} + H_{\mathbf{k}}^{(+1)} e^{i\omega t} + H_{\mathbf{k}}^{(-1)} e^{-i\omega t}, \quad (48)$$

or we can consider $\bar{H}_{\mathbf{k}}$ from Eq. (42), which describes the insulating phase dynamically produced by the first order correction in ω^{-1} .

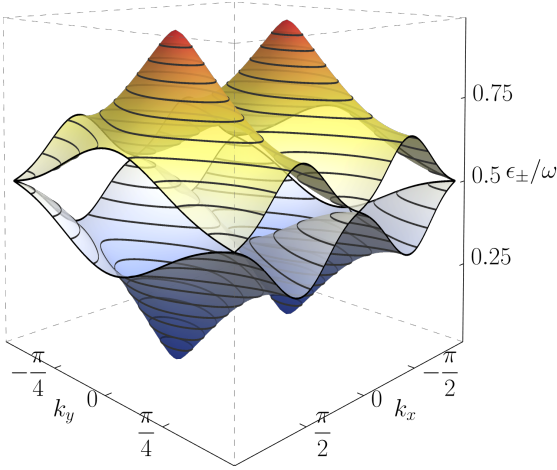


FIG. 9. Quasienergy spectrum centered at the π -gap for PBC and the frequency given by the resonance condition from Eq. (56). The 0-gap remains open due to the dynamical gap, but the π -gap exactly closes at $\mathbf{k} = (0, \pm\pi/2)$, producing a topological phase transition that changes the Chern number. Parameters: $A_x = 0.5$, $A_y = 0.5$ and $\varphi = \pi/2$.

Strictly speaking, the correct choice is the first one. This is to be expected, and we have checked that the numerical solution of Eq. (48) perfectly agrees with the numerical solution of the full time-dependent Hamiltonian, for the case of moderate field amplitudes. However, it turns out that it is not compatible with the successive RWA. *This is because neglecting counter-rotating terms to capture the resonance is only correct near the resonance, but not at high frequency, where rotating and counter-rotating terms contribute similar amounts.* In particular, one finds that applying the RWA to Eq. (48) results in an incorrect mass term at high frequency, and crucially, does not open the 0-gap. For this reason, the first choice gives an erroneous band structure where the π -gap is correctly captured from the RWA, but the 0-gap remains closed, because it is generated from the rotating terms only. This can be fixed using more sophisticated theoretical methods [33, 34, 62], but in order to avoid the use of heavier numerical calculations, let us justify the range of validity of the second option.

If we consider the static part to be given by $\bar{H}_{\mathbf{k}}$ instead of $H_{\mathbf{k}}^{(0)}$, the time-dependent Hamiltonian becomes (cf. Eq. (48)):

$$H_{\mathbf{k}}(t) \approx \bar{H}_{\mathbf{k}} + H_{\mathbf{k}}^{(+1)} e^{i\omega t} + H_{\mathbf{k}}^{(-1)} e^{-i\omega t}. \quad (49)$$

As previously mentioned, there is a redundancy in $H_{\mathbf{k}}(t)$, because the effect of the rotating and counter-rotating terms at high frequency is already included in $\bar{H}_{\mathbf{k}}$. However, we can see that the effect of the driving is quite different in resonant and off-resonant states.

In particular, the high frequency correction strongly modifies the quasienergy band structure near the Dirac points at the 0-gap, leaving the rest of the band structure

mostly unaffected (cf. Fig. 7, panel (b), and Fig. 8, panel (a)). Also, in the Appendix B, Fig. 12, we plot the overlap of the two band structures for direct comparison). In contrast, the states that are resonant mainly modify the π -gap. This means that if the frequency is larger than the gap opened by the mass term, but smaller than the bandwidth, we can separate the off-resonant effect for states near the Dirac points (0-gap opening), from the resonance effect at higher energy states, away from the Dirac points (π -gap opening). See Fig. 7, panel (c) for a schematic description of the energy scales involved.

Therefore, we can conclude that the approximation will be more accurate for systems with a large bandwidth, and with drive frequencies ω , larger than the dynamical gap:

$$4\sqrt{J_{x,0}^2 + J_{y,0}^2} \gg \omega \gg 16J_{x,1}J_{y,1}/\omega. \quad (50)$$

Under this condition, the physics of states at resonance and off-resonance is effectively decoupled and Eq. (49) provides a good approximation. Importantly, notice that as the dynamical gap size depends on the field amplitude A_u , the approximation at a given frequency can usually be improved by lowering the amplitude. The reason is that a smaller amplitude reduces the size of the region of states affected by the gap opening and then, enlarges the energy separation between resonant and off-resonant states.

Now we perform a similar analysis as for SSH chain in the previous section. First, we transform the time-dependent Hamiltonian from Eq. (49) to the basis of eigenstates of $\bar{H}_{\mathbf{k}}$:

$$\hat{H}_{\mathbf{k}}(t) = D(\mathbf{k}) + \hat{V}(\mathbf{k}, t), \quad (51)$$

with

$$\hat{V}(\mathbf{k}, t) = \Lambda^\dagger(\mathbf{k}) \left[H_{\mathbf{k}}^{(+1)} e^{i\omega t} + H_{\mathbf{k}}^{(-1)} e^{-i\omega t} \right] \Lambda(\mathbf{k}) \quad (52)$$

and $D(\mathbf{k})$ a diagonal matrix with entries given by the energies in Eq. (46). Next, we isolate the rotating terms, which requires to keep only the term proportional to σ_- from $H_{\mathbf{k}}^{(+1)}$, and the term proportional to σ_+ from $H_{\mathbf{k}}^{(-1)}$. With this, we arrive to the final RWA Hamiltonian:

$$H_{\text{RWA}}(\mathbf{k}, t) = \begin{pmatrix} E_+(\mathbf{k}) & \hat{V}(\mathbf{k})^{1,2} e^{-i\omega t} \\ \hat{V}(\mathbf{k})^{2,1} e^{i\omega t} & E_-(\mathbf{k}) \end{pmatrix}. \quad (53)$$

The solution to the time-dependent Schrödinger equation is straightforward to obtain by means of a transformation $R(t) = e^{-i\frac{\omega}{2}t\sigma_z}$, which results in the following rotating frame Hamiltonian:

$$\tilde{H}_{\mathbf{k}} = \begin{pmatrix} E_+(\mathbf{k}) - \frac{\omega}{2} & \Gamma(\mathbf{k}) \\ \Gamma(\mathbf{k})^* & E_-(\mathbf{k}) + \frac{\omega}{2} \end{pmatrix}, \quad (54)$$

with eigenvalues

$$\tilde{E}_{\pm}(\mathbf{k}) = \pm \sqrt{\left[E_+(\mathbf{k}) - \frac{\omega}{2} \right]^2 + |\Gamma(\mathbf{k})|^2}, \quad (55)$$

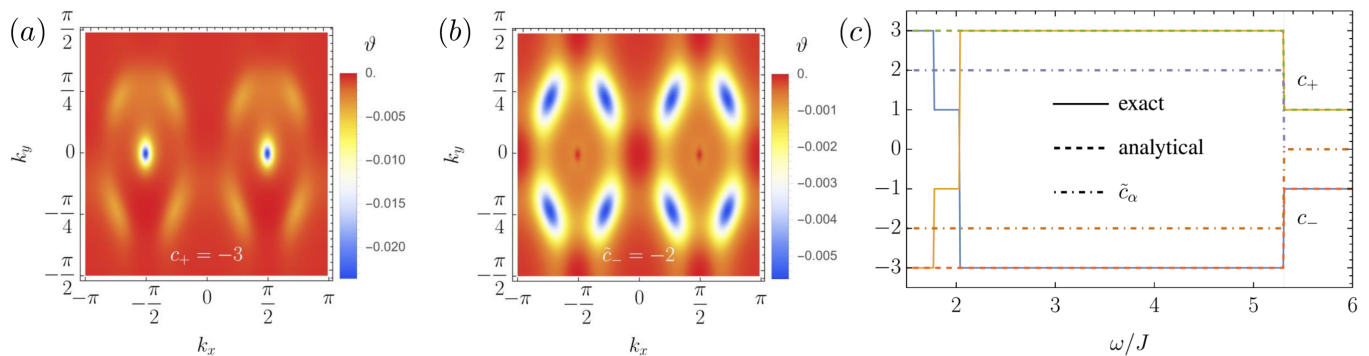


FIG. 10. (a) Berry flux distribution for the upper quasienergy band for a frequency below a resonant configuration, $\omega = 3.5J$, with Chern number $c_+ = -3$. (b) Berry flux for the rotating frame Hamiltonian for identical parameters. (c) Chern number as a function of frequency for identical conditions as panel (a). Parameters: $\varphi = \pi/2$ and $A_x = A_y = 0.5$.

being $\Gamma(\mathbf{k}) \equiv \hat{V}(\mathbf{k})^{1,2} = [\hat{V}(\mathbf{k})^{2,1}]^*$. Formally, this solution is similar to that of the SSH chain in Eq. (31), and we expect a topological phase transition due to a resonance if the gap closes at particular points of the FBZ.

In particular, the requirements for a gap closure are obtained from Eq. (55), and correspond to the resonance condition, $\omega = 2E_+(\mathbf{k})$, and the exact degeneracy condition, $\Gamma(\mathbf{k}) = 0$. In the Appendix A is shown a general method to solve for them and it is demonstrated that, in the present case, the π -gap closes at $\mathbf{k} = (0, \pm\pi/2)$. At these points the mass term identically vanishes and the resonance condition reduces to:

$$\omega = 4\sqrt{J_{x,0}^2 + J_{0,y}^2}. \quad (56)$$

In Fig. 9 we plot the quasienergy spectrum centered at the π -gap, for a frequency that fulfills the resonance condition in Eq. (56). It shows that the π -gap exactly closes at $\mathbf{k} = (0, \pm\pi/2)$, as predicted above. Also, one can see that the 0-gap remains open due to the off-resonant contributions, confirming the energy scale separation between resonant and off-resonant degrees of freedom.

C. Topology induced by resonances

Once we have confirmed that the quasienergy band structure is correctly captured by our RWA effective Hamiltonian, we move on to analyze the topological properties of the bands. In particular, as we are interested in changes in the topology as the frequency is lowered, we focus on the effect of the resonance in the Chern number. For that, let us first study the Berry flux distribution. It is an interesting quantity because it can be measured experimentally [17], and because its integral over the FBZ is proportional to the Chern number.

For PBC, one can calculate the Berry flux distribution numerically, by discretizing the FBZ, finding the Berry flux along each plaquette and plotting its value over all plaquettes. The Berry flux piercing a single plaquette is

just the angle rotated by an eigenstate during parallel transport in momentum space [63]:

$$\vartheta_\alpha(\mathbf{k}) = -\text{Im} \left\{ \log \left[\frac{\langle \Phi_\alpha(k_x, k_y) | \Phi_\alpha(k_x + \delta k_x, k_y) \rangle \langle \Phi_\alpha(k_x + \delta k_x, k_y) | \Phi_\alpha(k_x + \delta k_x, k_y + \delta k_y) \rangle \langle \Phi_\alpha(k_x + \delta k_x, k_y + \delta k_y) | \Phi_\alpha(k_x, k_y + \delta k_y) \rangle \langle \Phi_\alpha(k_x, k_y + \delta k_y) | \Phi_\alpha(k_x, k_y) \rangle}{\langle \Phi_\alpha(k_x, k_y) | \Phi_\alpha(k_x, k_y) \rangle} \right] \right\}. \quad (57)$$

The Chern number is obtained by calculating the total flux:

$$c_\alpha = \frac{1}{2\pi} \sum_{\mathbf{k} \in \text{FBZ}} \vartheta(\mathbf{k})_\alpha. \quad (58)$$

Obviously, for the case of Floquet states, $\Phi_\alpha(\mathbf{k}, t)$, the Berry flux and the Chern number will inherit a time dependence. However, this will be irrelevant for our case, as it only shifts the Berry flux in momentum space, but does not affect the total sum over the FBZ. Hence, we find that the resulting Chern number is time-independent.

First, we calculate the Berry flux distribution and the Chern number for the exact Floquet bands $\epsilon_\alpha(\mathbf{k})$. If we focus on the high frequency regime, the calculation of the Berry flux results in the plot shown in Fig. 8, panel (c). As expected, the Berry flux is mostly located around the Dirac points and perfectly agrees with the flux obtained from the stroboscopic effective Hamiltonian $\bar{H}_\mathbf{k}$, in Eq. (42). Analogously, the sum results in a Chern number in perfect agreement with the number of edge states present in the 0-gap of the high frequency regime. Therefore, we can conclude that the high frequency analysis for the 0-gap topology nicely agrees with the exact numerical results, and the Berry flux distribution is faithfully reproduced.

As the frequency is lowered and the picture of stroboscopic dynamics breaks down, the Berry flux changes, but it can still be calculated numerically for the Floquet states. This gives us some information about the topology, but as previously discussed, the number of edge states is not generally proportional to the value of this Chern number [12]. In particular, let us consider a situation where the driving frequency is below the resonance

indicated by Eq. (56). The corresponding Berry flux distribution, for the top Floquet band, is shown in Fig. 10, panel (a). Interestingly, the Berry flux still is large near the original position of the Dirac points. However, on top of this, there is an additional contribution distributed over a much wider area around them. The calculation of the Chern number gives in this case $c_+ = -3$, which indicates that the additional contribution to the flux, due to its large extension, changes the Chern number in two units. Also, we can conclude that because $c_{\pm} \neq 0$, the phase including a resonance is not anomalous in this case. However, this is not important, as we are interested in the possibility to separate the topology of Floquet phases in general, not only for the anomalous case.

Now let us check if our analytical solution for the Floquet states can shed light onto the number of edge states at each gap, without calculating the spectrum for OBC. The general expression for the Floquet states in the zero sideband, under the RWA, reads:

$$|\Phi_{\pm}(\mathbf{k}, t)\rangle = \Lambda(\mathbf{k}) e^{-i\frac{\omega}{2}t(\sigma_z \mp 1)} |\phi_{\pm}(\mathbf{k})\rangle. \quad (59)$$

We know that the relevant invariant for this system is the Chern number, and as for the case of the SSH chain, the Eq. (59) can be separated in two contributions: the one from the rotating frame Hamiltonian, and the one from the renormalized bands in the high frequency regime:

$$c_{\alpha} = \tilde{c}_{-\alpha} + \bar{c}_{-\alpha}, \quad (60)$$

with \tilde{c}_{α} the Chern number for the band α of the rotating frame Hamiltonian, and \bar{c}_{α} the contribution from the transformation $\Lambda(\mathbf{k})$ to that band [64].

First, we calculate the total Berry flux distribution from the analytical expression of the Floquet states in Eq. (59), and find that the agreement with the numerical value of the Berry flux from the full Hamiltonian is excellent. Next, we calculate the Berry flux distribution of the eigenstates $|\phi_{\pm}(\mathbf{k})\rangle$ of the rotating frame Hamiltonian $\tilde{H}_{\mathbf{k}}$. Its value is shown in Fig.10, panel (b), and when combined with the high frequency contribution shown in Fig.8, panel (c), it perfectly reproduces the total Berry flux in Fig.10, panel (a) (for the comparison, notice the difference in scale between panels (a) and (b) in Fig. 10). This means that the Berry flux of the Floquet states can be separated in two time-independent contributions, one coming from the high frequency Hamiltonian $\tilde{H}_{\mathbf{k}}$, and another coming from the rotating frame Hamiltonian $\tilde{H}_{\mathbf{k}}$. On top of this, the corresponding Chern number \tilde{c}_{α} predicts a change in two units at the π -gap, in perfect agreement with the change in the total Chern number calculated from the exact Floquet states. This indicates that the RWA approximation for the Floquet states captures the relevant changes in the topology, and confirms that, in analogy with the one-dimensional example, it can be separated in two contributions, one for each frame of reference, or equivalently, for each nonequivalent gap.

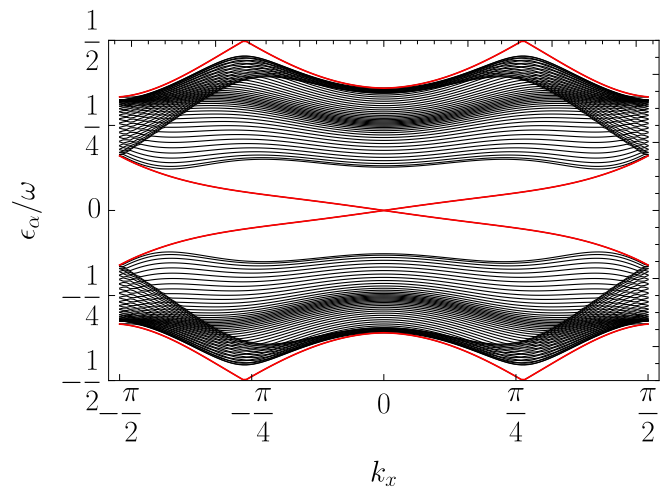


FIG. 11. Quasienergy spectrum for OBC along the y -axis for the same parameters as those used in Fig. 10. The chiral edge states are highlighted in red.

Let us now check the range of validity of our analytical solution. In particular we are interested in its breakdown as the frequency is lowered and the states at low energy become resonant. In Fig.10, panel (c), we plot the value of the Chern number from the full Hamiltonian, as a function of frequency. One can see that the analytical (dashed) and the exact (solid) perfectly agree at high and intermediate frequency. Furthermore, the critical frequency $\omega \simeq 5.3J$, for the topological phase transition predicted from Eq. (56) perfectly reproduces the exact critical point (vertical grey line). At even lower frequencies, of the order of $\omega = 2J$, there is a disagreement, but this is to be expected due to the resonance of states near the Dirac points, which are heavily affected by the dynamical gap.

We also plot the value for the Chern number in the rotating frame \tilde{c}_{α} , which shows that its change is the one that controls the change in the topological phase, while the 0-gap remains unaffected. This confirms that for the frequency range $\omega \in [2J, 5.3J]$, the resonance produces the topological changes.

As a final check, we consider OBC and plot in Fig. 11 the quasienergy spectrum for a ribbon with boundary along the y -axis. It shows that, as predicted, the 0-gap hosts a pair of edge states (red), while simultaneously in the π -gap there are two pairs of edge states, consequence of the topological phase transition triggered by the resonance. This shows that we have correctly predicted the number of edge states in each gap, and that they are of topological origin. Furthermore, we have checked that they also appear for OBC along the x -axis, indicating that the boundary-dependence of the undriven phase is irrelevant in this topological phase. Therefore, our results confirm that the bulk-to-edge correspondence at each gap, previously obtained for the one-dimensional case in terms of different frames of reference, is also valid in two-dimensions.

V. CONCLUSIONS:

In this work we have discussed the importance of resonance phenomena in Floquet phases, and in particular, its crucial role in the existence of anomalous topology. For that, we have provided a novel and physically intuitive approach to understand Floquet topological phases, which is valid from the high to the resonant frequency regime. It shows that the topology of periodically driven systems can be systematically mapped to an effective RWA Hamiltonian, where the relation between physical processes and topology is very transparent. On the one hand, it demonstrates that the topology of Floquet systems can be understood as the one of the 0-gap topology, which is captured by a high frequency effective Hamiltonian, and the one of the π -gap topology, which is related with the resonance mechanism, only activated at lower frequencies. That is why in the literature, the latter always involves the micromotion. However, notice that with this framework we avoid the use of logarithm branch-cuts.

Importantly, our derivation of the RWA effective Hamiltonian generalizes the well known high frequency expansion of Floquet engineering, and by including the role of resonances, the transition between different frequency regimes can be continuously studied. On top of this, we have obtained analytical solutions for the Floquet states of the driven SSH chain and the π -flux lattice that encode the effect of rotating, counter-rotating terms and resonances in their topology.

From a topological perspective, the separation of topological invariants in different frames of reference allows to

understand the bulk-to-edge correspondence in Floquet systems from a different perspective and simplifies the calculations of some invariants.

These results are not only important from a theoretical perspective, but also for experimental setups, as usually the description of a system with driving involves both, resonant and off-resonant states, and one cannot restrict the theory to a high frequency expansion only. They allow to predict the necessary conditions for exact gap closures, based on the symmetries of the driving and lattice, and to determine the particular frequency values required for this to happen.

These results also open new horizons for future work. On the experimental side, it is possible to measure the Berry flux curvature very accurately [65], but as shown in this work, Floquet systems mix the contribution from both frames of reference. Therefore, by knowing the RWA Hamiltonian and its flux distribution, it should be possible to extract from the experiment the two contributions and discriminate anomalous Floquet phases from their trivial counterparts by direct measurement of the Berry flux [66].

ACKNOWLEDGMENTS

We acknowledge P. Delplace, A. Amo, B. Pérez-González, G. Platero and R. Molina their useful comments and the critical reading of the manuscript. We also acknowledge support from the European Union's Horizon2020 research and innovation program under Grant Agreement No.899354 (SuperQuLAN) and from CSIC Interdisciplinary Thematic Platform (PTI+) on Quantum Technologies (PTI-QTEP+).

-
- [1] S. Sachdev, *Quantum Phase Transitions*, 2nd ed. (Cambridge University Press, 2011).
- [2] A. Y. Kitaev, *Physics-Uspekhi* **44**, 131 (2001).
- [3] P. Delplace, J. B. Marston, and A. Venaille, *Science* **358**, 1075 (2017).
- [4] A. Leclerc, G. Laibe, P. Delplace, A. Venaille, and N. Perez, *ApJ* **940**, 84 (2022).
- [5] T. Oka and H. Aoki, *Phys. Rev. B* **79**, 081406 (2009).
- [6] T. Kitagawa, E. Berg, M. Rudner, and E. Demler, *Phys. Rev. B* **82**, 235114 (2010).
- [7] N. H. Lindner, G. Refael, and V. Galitski, *Nature Phys* **7**, 490 (2011).
- [8] A. G. Grushin, A. Gómez-León, and T. Neupert, *Physical Review Letters* **112**, 156801 (2014).
- [9] A. Díaz-Fernández, E. Díaz, A. Gómez-León, G. Platero, and F. Domínguez-Adame, *Phys. Rev. B* **100**, 075412 (2019).
- [10] M. S. Rudner, N. H. Lindner, E. Berg, and M. Levin, *Phys. Rev. X* **3**, 031005 (2013).
- [11] A. Gómez-León and G. Platero, *Physical Review Letters* **110**, 200403 (2013).
- [12] A. Gómez-León, P. Delplace, and G. Platero, *Phys. Rev. B* **89**, 205408 (2014).
- [13] L. E. F. Foa Torres, P. M. Perez-Piskunow, C. A. Balseiro, and G. Usaj, *Phys. Rev. Lett.* **113**, 266801 (2014).
- [14] A. Gómez-León, T. Ramos, A. González-Tudela, and D. Porras, *Phys. Rev. A* **106**, L011501 (2022).
- [15] T. Bessho and M. Sato, *Phys. Rev. Lett.* **127**, 196404 (2021), publisher: American Physical Society.
- [16] Y. H. Wang, H. Steinberg, P. Jarillo-Herrero, and N. Gedik, *Science* **342**, 453 (2013), <https://www.science.org/doi/pdf/10.1126/science.1239834>.
- [17] K. Wintersperger, C. Braun, F. N. Ünal, A. Eckardt, M. D. Liberto, N. Goldman, I. Bloch, and M. Aidelsburger, *Nature Physics* **16**, 1058 (2020).
- [18] M. C. Rechtsman, J. M. Zeuner, Y. Plotnik, Y. Lumer, D. Podolsky, F. Dreisow, S. Nolte, M. Segev, and A. Szameit, *Nature* **496**, 196 (2013).
- [19] Q. Cheng, Y. Pan, H. Wang, C. Zhang, D. Yu, A. Gover, H. Zhang, T. Li, L. Zhou, and S. Zhu, *Phys. Rev. Lett.* **122**, 173901 (2019).
- [20] Z. Cheng, R. W. Bomantara, H. Xue, W. Zhu, J. Gong, and B. Zhang, *Phys. Rev. Lett.* **129**, 254301 (2022).
- [21] L. K. Upreti, C. Evain, S. Randoux, P. Suret, A. Amo, and P. Delplace, *Phys. Rev. Lett.* **125**, 186804 (2020).
- [22] A. F. Adiyatullin, L. K. Upreti, C. Lechevalier, C. Evain, F. Copie, P. Suret, S. Randoux, P. Delplace, and A. Amo, *Phys. Rev. Lett.* **130**, 056901 (2022).

- [23] J. W. McIver, B. Schulte, F. U. Stein, T. Matsuyama, G. Jotzu, G. Meier, and A. Cavalleri, *Nature Physics* **16**, 38 (2019).
- [24] F. Nathan and M. S. Rudner, *New Journal of Physics* **17**, 125014 (2015).
- [25] M. S. Rudner and N. H. Lindner, *Nat Rev Phys* **2**, 229 (2020).
- [26] M. Nakagawa, R.-J. Slager, S. Higashikawa, and T. Oka, *Phys. Rev. B* **101**, 075108 (2020).
- [27] I. I. Rabi, *Phys. Rev.* **51**, 652 (1937).
- [28] A. Gómez-León and G. Platero, *Phys. Rev. B* **84**, 121310 (2011).
- [29] A. Gómez-León and G. Platero, *Phys. Rev. B* **85**, 245319 (2012).
- [30] P. Delplace, A. Gómez-León, and G. Platero, *Phys. Rev. B* **88**, 245422 (2013).
- [31] F. Grossmann, T. Dittrich, P. Jung, and P. Hänggi, *Phys. Rev. Lett.* **67**, 516 (1991).
- [32] M. Grifoni and P. Hänggi, *Physics Reports* **304**, 229 (1998).
- [33] M. Vogl, P. Laurell, A. D. Barr, and G. A. Fiete, *Physical Review X* **9**, 021037 (2019).
- [34] S. J. Thomson, D. Magano, and M. Schirò, *SciPost Phys.* **11**, 028 (2021).
- [35] A. Eckardt and E. Anisimovas, *New Journal of Physics* **17**, 093039 (2015).
- [36] R. Peierls, *Zeitschrift für Physik* **80**, 763 (1933).
- [37] G. H. Wannier, *Rev. Mod. Phys.* **34**, 645 (1962).
- [38] T. Kitagawa, M. A. Broome, A. Fedrizzi, M. S. Rudner, E. Berg, I. Kassal, A. Aspuru-Guzik, E. Demler, and A. G. White, *Nat Commun* **3**, 882 (2012).
- [39] Single-band models could also display resonant transitions, but only if the driving field is not spatially homogeneous and can couple states with different momentum.
- [40] W. P. Su, J. R. Schrieffer, and A. J. Heeger, *Phys. Rev. Lett.* **42**, 1698 (1979).
- [41] B. Pérez-González, M. Bello, A. Gómez-León, and G. Platero, *Phys. Rev. B* **99**, 035146 (2019).
- [42] B. Pérez-González, M. Bello, G. Platero, and A. Gómez-León, *Phys. Rev. Lett.* **123**, 126401 (2019).
- [43] V. Dal Lago, M. Atala, and L. E. F. Foa Torres, *Phys. Rev. A* **92**, 023624 (2015).
- [44] O. Balabanov and H. Johannesson, *Phys. Rev. B* **96**, 035149 (2017), publisher: American Physical Society.
- [45] F. Cardano, A. D’Errico, A. Dauphin, M. Maffei, B. Piccirillo, C. de Lisio, G. De Filippis, V. Cataudella, E. Santamato, L. Marrucci, M. Lewenstein, and P. Massignan, *Nat Commun* **8**, 15516 (2017).
- [46] J. K. Asbóth, B. Tarasinski, and P. Delplace, *Phys. Rev. B* **90**, 125143 (2014).
- [47] The springs could be phonons in some realizations, if their frequency is in the correct range of energies.
- [48] A. Gómez-León and G. Platero, *Physical Review Research* **2**, 033412 (2020).
- [49] A. Gómez-León, *Phys. Rev. A* **106**, 022609 (2022).
- [50] Y. Aharonov and J. Anandan, *Phys. Rev. Lett.* **58**, 1593 (1987).
- [51] Although the first contribution to Eq. (36) is time-dependent, its evaluation turns out to be time-independent.
- [52] Y.-X. Zhang, H.-M. Guo, and R. T. Scalettar, *Phys. Rev. B* **101**, 205139 (2020).
- [53] M. Rodríguez-Vega, A. Kumar, and B. Seradjeh, *Phys. Rev. B* **100**, 085138 (2019).
- [54] B. A. Bernevig and T. L. Hughes, *Topological Insulators and Topological Superconductors* (Princeton University Press, Princeton and Oxford, 2013).
- [55] P. Delplace, D. Ullmo, and G. Montambaux, *Phys. Rev. B* **84**, 195452 (2011).
- [56] R. Roy and F. Harper, *Physical Review B* **96**, 155118 (2017).
- [57] S. A. Sato, J. W. McIver, M. Nuske, P. Tang, G. Jotzu, B. Schulte, H. Hübener, U. De Giovannini, L. Mathey, M. A. Sentef, A. Cavalleri, and A. Rubio, *Phys. Rev. B* **99**, 214302 (2019).
- [58] S. Ryu, A. P. Schnyder, A. Furusaki, and A. W. W. Ludwig, *New Journal of Physics* **12**, 065010 (2010).
- [59] C.-K. Chiu, J. C. Teo, A. P. Schnyder, and S. Ryu, *Reviews of Modern Physics* **88**, 035005 (2016).
- [60] D. Sticlet, F. Piéchon, J.-N. Fuchs, P. Kalugin, and P. Simon, *Phys. Rev. B* **85**, 165456 (2012).
- [61] We have checked that this simplified Hamiltonian perfectly reproduces the exact quasienergies of the full model, for the range of parameters of interest.
- [62] Z. Lü and H. Zheng, *Phys. Rev. A* **86**, 023831 (2012).
- [63] T. Fukui, Y. Hatsugai, and H. Suzuki, *Journal of the Physical Society of Japan* **74**, 1674 (2005), <https://doi.org/10.1143/JPSJ.74.1674>.
- [64] Importantly, remember that as for the SSH chain, the band index of the rotating frame Hamiltonian and that of the quasienergies is reversed in order. That is why the $\tilde{c}_{-\alpha}$ is the π -gap contribution to the Chern number c_{α} .
- [65] C. Lechevalier, C. Evain, P. Suret, F. Copie, A. Amo, and S. Randoux, *Communications Physics* **4**, 243 (2021).
- [66] R. E. Sokhen, Álvaro Gómez-León, A. F. Adiyatullin, S. Randoux, P. Delplace, and A. Amo, *Discrete step walks reveal unconventional anomalous topology in synthetic photonic lattices* (2023), arXiv:2311.10619 [cond-mat.mes-hall].

Appendix A: General analysis of RWA Hamiltonian

To find a general expression for the exact degeneracy condition of the RWA Hamiltonian, in a two-level system, we can write the eigenstates in the following generalized form:

$$|v_+\rangle = \begin{pmatrix} \cos\left(\frac{\theta}{2}\right) e^{-i\phi} \\ \sin\left(\frac{\theta}{2}\right) \end{pmatrix}, \quad |v_-\rangle = \begin{pmatrix} \sin\left(\frac{\theta}{2}\right) e^{-i\phi} \\ -\cos\left(\frac{\theta}{2}\right) \end{pmatrix} \quad (\text{A1})$$

Hence, the transformation matrix to the diagonal basis is:

$$\Lambda = \begin{pmatrix} \cos\left(\frac{\theta}{2}\right) e^{-i\phi} & \sin\left(\frac{\theta}{2}\right) e^{-i\phi} \\ \sin\left(\frac{\theta}{2}\right) & -\cos\left(\frac{\theta}{2}\right) \end{pmatrix} \quad (\text{A2})$$

Now, consider for example the π -flux lattice of this work. Taking into account that the driving term under the assumption of moderate driving is:

$$H_{\mathbf{k}}^{(\pm 1)} = \begin{pmatrix} 0 & V_{\pm}^{1,2} \\ V_{\pm}^{2,1} & 0 \end{pmatrix} \quad (\text{A3})$$

with

$$V_{\pm}^{1,2} = \pm 2 [iJ_{x,1} \sin(k_x) - J_{y,1} e^{\pm i\varphi} \cos(k_y)] \quad (\text{A4})$$

and

$$V_{\pm}^{2,1} = \pm 2 [iJ_{x,1} \sin(k_x) + J_{y,1} e^{\pm i\varphi} \cos(k_y)], \quad (\text{A5})$$

the transformation to the diagonal basis gives:

$$\Lambda^\dagger H_{\mathbf{k}}^{(\pm 1)} \Lambda = \frac{1}{2} \begin{pmatrix} \sin(\theta) \left(e^{-i\varphi} V_{\pm}^{2,1} + e^{i\varphi} V_{\pm}^{1,2} \right) & e^{-i\varphi} V_{\pm}^{2,1} [1 - \cos(\theta)] - e^{i\varphi} V_{\pm}^{1,2} [1 + \cos(\theta)] \\ e^{i\varphi} V_{\pm}^{1,2} [1 - \cos(\theta)] - e^{-i\varphi} V_{\pm}^{2,1} [1 + \cos(\theta)] & -\sin(\theta) \left(e^{-i\varphi} V_{\pm}^{2,1} + e^{i\varphi} V_{\pm}^{1,2} \right) \end{pmatrix} \quad (\text{A6})$$

From this expression, we can extract the rotating and counter-rotating terms:

$$\Gamma(\mathbf{k}) = \frac{1}{2} e^{-i\varphi} V_{-}^{2,1} [1 - \cos(\theta)] - \frac{1}{2} e^{i\varphi} V_{-}^{1,2} [1 + \cos(\theta)] = \frac{1}{2} e^{i\varphi} V_{+}^{1,2} [1 - \cos(\theta)] - \frac{1}{2} e^{-i\varphi} V_{+}^{2,1} [1 + \cos(\theta)] \quad (\text{A7})$$

Hence, the condition for exact degeneracy is $|\Gamma(\mathbf{k})|^2 = 0$. From that, we can already see that, for example, the degeneracy will happen if $V_{\pm}^{1,2} = V_{\pm}^{2,1} = 0$. Hence, as their \mathbf{k} -dependence goes as $\sin(k_x)$ and $\cos(k_y)$, we can conclude that the gap will exactly close at $\mathbf{k} = \pi(n, m + 1/2)$. Notice that this is completely independent of the field values, which indicates that it is purely an effect from the symmetries of the coupling term.

Appendix B: Additional results for the π -flux lattice

In the derivation of the RWA Hamiltonian for the two-dimensional semi-metal we have assumed that the effect of the driving can be separated into off-resonant and resonant states. For this to be true, we need that the dynamical gap opened by the high frequency contribution is small, compared with the energy splitting of the states resonantly coupled to the field. This is possible because the renormalization of the band due to off-resonant corrections dominates close to the Dirac points. This is shown in Fig. 12 where we compare the band before and after the high frequency field is applied. It can be seen that near the Dirac points the bands change considerably, but beyond a certain energy, the bands remain almost identical. Those are the states can be resonantly coupled by the drive in our approximation.

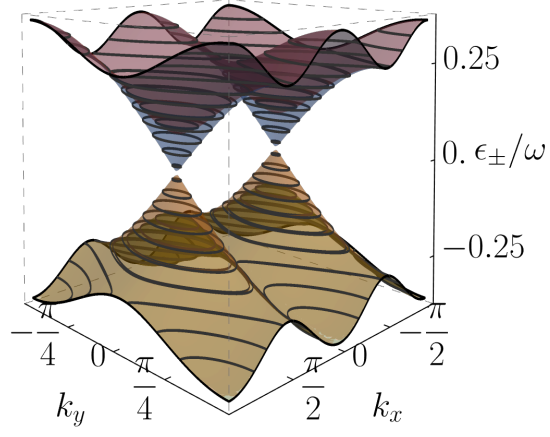


FIG. 12. Comparison between the band structure before and after the drive is applied. In blue and yellow we can see the original undriven bands with their Dirac cones. Underneath are plotted in red and green the driven bands. We have considered $\omega = 6J$, $A_{x,y}=1$ and $\varphi = \pi/2$.